Understanding of the oxygen activation on ceriaand ceria/alumina-supported gold catalysts: a study combining 18O/16O isotopic exchange and EPR spectroscopy

Pandian Lakshmanan, Frédéric Averseng, Nicolas Bion, Laurent Delannoy,
Jean-Michel Tatibouet, Catherine Louis

To cite this version:

Pandian Lakshmanan, Frédéric Averseng, Nicolas Bion, Laurent Delannoy, Jean-Michel Tatibouet, et al.. Understanding of the oxygen activation on ceriaand ceria/alumina-supported gold catalysts: a study combining 18O/16O isotopic exchange and EPR spectroscopy. Gold bulletin : a quarterly review of research on gold and its applications in industry, 2013, 46, pp.233-242. 10.1007/s13404-013-0103-z . hal-00961263

HAL Id: hal-00961263
https://hal.sorbonne-universite.fr/hal-00961263v1

Submitted on 23 Sep 2021

Gold Bull (2013) 46:233–242
DOI 10.1007/s13404-013-0103-z

ORIGINAL PAPER

Understanding of the oxygen activation on ceria- and ceria/alumina-supported gold catalysts: a study combining $^{18}O/^{16}O$ isotopic exchange and EPR spectroscopy

Pandian Lakshmanan · Frédéric Averseng · Nicolas Bion · Laurent Delannoy · Jean-Michel Tatibouët · Catherine Louis

Abstract Gold supported on ceria or ceria–alumina mixed oxides are very active catalysts for total oxidation of a variety of molecules. The key step of the oxygen activation on such catalysts is still a matter of debate. Gold–ceria (Au/CeO_2) and gold–ceria–alumina ($Au/CeO_2/Al_2O_3$) catalysts were prepared by deposition–precipitation of gold precursor with urea as in former works where their efficiency to catalyze the oxidation of propene and propan-2-ol was demonstrated. To understand the phenomenon of oxygen activation over this class of catalysts, efficient techniques generally used to characterize the interaction between oxygen and cerium-based oxides were applied; the oxygen storage capacity (OSC) measurement, the $^{18}O_2/^{16}O_2$ isotopic exchange study (OIE), as well as characterizations by in situ Raman and electron paramagnetic resonance (EPR) spectroscopies. Each of the techniques allowed showing the impact of the gold nanoparticles on the activation of dioxygen, on the kinetic governing the gas-phase/solid oxygen atom exchange, and on the nature and the location of the adsorbed oxygen species. Gold nanoparticles were shown to increase drastically the OSC values and the rate of oxygen exchange. OIE study demonstrated the absence of pure equilibration reaction ($^{16}O_{2(g)}+^{18}O_{2(g)} \leftrightarrow 2\ ^{16}O^{18}O_{(g)}$), indicating that gold did not promote the dissociation of dioxygen. Peroxo adspecies were observed by Raman spectroscopy only in the presence of gold. On the contrary, EPR spectroscopy indicated that the concentration of superoxo adspecies was lower for oxide-supported gold samples than for bare oxides. The combination of techniques allowed reinforcing the hypothesis that the gold nanoparticules promote the activation of dioxygen by generating extremely mobile diatomic-oxygenated species at the gold/ceria interfacial perimeter. This specific gold–ceria interaction, which leads to the increase in oxygen mobility, is probably also responsible for the higher catalytic performance of Au/CeO_2 and $Au/CeO_2/Al_2O_3$ in oxidation reaction compared to bare supports.

Keywords Gold · Heterogeneous catalysis · $^{18}O_2/^{16}O_2$ isotopic exchange · EPR · Raman · Ceria · Oxygen storage capacity · Oxygen species

Introduction

Since the exceptional discovery of Haruta who demonstrated that, when smaller than 5 nm, the gold nanoparticules can display very high catalytic CO oxidation activity even at 203 K [1, 2], hundreds of papers on the topic of catalysis by gold have been annually published with a progression which remains exponential. Then, numerous catalytic formulations have been developed, and the efficiency of nanostructured gold deposited on reducible transition metal oxide supports was particularly reported [3]. Among the reducible oxide supports, ceria was particularly investigated because of its capability to act as an oxygen reservoir by storing/releasing oxygen through a redox process which involves the Ce^{4+}/Ce^{3+} couple. Nanocrystalline ceria-supported gold catalysts were then studied in various catalytic reactions including the water–gas shift reaction [4, 5], the VOC combustion [6–10], the selective oxidation of alcohol [11], the selective oxidation of CO in excess of H_2 (CO-PROX) [12], and the most investigated reaction remaining the low-temperature CO oxidation [13, 14]. The morphology of

---

Electronic supplementary material The online version of this article (doi:10.1007/s13404-013-0103-z) contains supplementary material, which is available to authorized users.

P. Lakshmanan · F. Averseng · L. Delannoy · C. Louis
Laboratoire de Réactivité de Surface, UMR 7197 CNRS, Université Pierre et Marie Curie-UMPC, 4 place Jussieu, 75252 Paris Cedex 05, France

P. Lakshmanan · N. Bion (✉) · J.-M. Tatibouët
CNRS UMR 7285, Institut de Chimie des Milieux et Matériaux de Poitiers (IC2MP), University of Poitiers, 4 rue Michel Brunet, 86022 Poitiers Cedex, France
e-mail: nicolas.bion@univ-poitiers.fr

the ceria crystallites, the size of the gold clusters (particles), and the oxidation state of the active gold atoms are the parameters usually discussed because of their determining importance for the catalytic oxidation activity [15]. The nature of the intermediate species is also studied. For instance, it has been clearly demonstrated that one of the key elements for explaining the high reactivity of nanometer-sized gold nanoparticles in CO oxidation was the abundance of low-coordinated Au atoms in the small particles, where CO can be preferentially adsorbed [16]. On the contrary, the nature of the intermediate species in the oxygen activation step is still a matter of debate [17]. One reason is the fact that the adsorbed oxygen species are not experimentally easy to identify in the conditions of the reaction. Some recent papers showed that the anion photoelectron spectroscopy [18] and infrared multiple photon dissociation [19] allowed determining which oxygenated species are involved in the activation process, but these spectroscopic studies have not been applied to ceria-supported gold catalysts. Computational method is a way to get around the experimental limitations, and very impressive demonstrations in terms of reactive intermediate species and mechanism scheme were reported [17, 20]. Nevertheless, the use of the theoretical modeling did not permit to prevent controversial conclusions.

In this work, we used a combination of characterization techniques involving oxygen storage capacity measurement (OSC), oxygen isotopic exchange (OIE), and Raman and electron paramagnetic resonance (EPR) spectroscopies. These techniques were extensively used on cerium-based oxides to understand the mechanism of dioxygen activation [21–23] and to explain the property of these oxides to store and release oxygen [24, 25]. Thus, we proposed to apply the same techniques on ceria-supported gold catalysts. In addition, gold supported on mixed oxide consisting of cerium oxide supported on alumina with two CeO_2 loadings (5 to 10 wt.%) were also studied. The latter catalytic formulations showed interesting catalytic performances in the oxidation of two types of VOCs as follows: propene [7] as model of hydrocarbon and 2-propanol [26] as model of alcohol. Ceria–alumina was preferred to ceria support because of the poor resistance of the latter against thermal sintering.

Experimental part

Materials

Alumina, AluC Degussa (110 $m^2\ g^{-1}$), was used as the support to load cerium oxide (5 and 10 wt.% with respect to alumina) by impregnation in excess of aqueous solution of $Ce(NO_3)_3$, $6H_2O$ (Aldrich, 99.9 %), followed by calcination at 500 °C. One weight percent of gold was loaded by deposition–precipitation with urea on the various CeO_2–Al_2O_3 samples as well as on pure alumina and ceria of high surface area (HSA-5 Rhodia, 200 $m^2\ g^{-1}$) and low surface area, sintered HSA-5 by aging at 800 °C under a flow of humid air for 12 h (abbreviated as CeO_2 LSA 50 $m^2\ g^{-1}$). The catalysts are named as Au/xCeO_2/Al_2O_3 (x=wt% of CeO_2), Au/Al_2O_3, and Au/CeO_2. The details of experimental procedures regarding catalyst preparation and characterization by elemental analyses, N_2 physisorption at 77 K, XRD, X-ray photoelectron spectroscopy (XPS), and combined TEM–energy-filtered transmission electron microscopy (EFTEM) techniques were largely described in our previous study [7].

Oxygen storage capacity

OSC measurements were carried out at 673 K using a U-form reactor connected to a gas chromatograph equipped with a Porapak column and a thermal conductivity detector. The experimental set-up and the protocol of experiment were reported elsewhere [27]. The samples were placed into the reactor and heated under a continuous flow of helium (30 $cm^3\ min^{-1}$) up to 673 K for 30 min before pretreatment with ten pulses (0.246 cm^3) of pure O_2 at atmospheric pressure followed by a purge with pure He for 10 min. Alternate pulses of CO and O_2 were undertaken three times in order to check the reproducibility of the measurement. The amounts of unconverted CO and O_2 as well as of produced CO_2 were quantified. The OSC was calculated from the average value of CO_2 production (after CO pulse) and was expressed in μmol O g^{-1} or μmol O m^{-2} taking into account the mass or the BET surface area of the samples.

The number of surface oxygen atoms involved in the OSC process was calculated considering that only ceria participated and assuming a preferential (100) orientation of the ceria surface. Calculations have been already described in a previous publication [27].

Oxygen isotopic exchange

OIE experiments were performed in a set-up already described elsewhere [27, 28]. A U-form reactor was placed in a closed recycle system which was connected on one side to a mass spectrometer (Pfeiffer Vacuum, QMS 200) for the monitoring of the gas-phase composition and on the other side to a vacuum pump. A recycling pump removed limitations due to gas-phase diffusion. OIE experiments were undertaken on 20 mg of catalyst, subjected to a $^{16}O_2$ activation step at 873 K under atmospheric pressure for 1 h prior to cooling to the desired temperature, at which point the system was degassed and the isotopic mixture charged. The study of homo-exchange (also called equilibration reaction) was performed using an equimolar mixture of $^{16}O_2$ and $^{18}O_2$ (99.9 % purity, supplied by Isotec), whereas for the study of the hetero-exchange, the mixture was replaced by pure $^{18}O_2$. The masses 32, 34, and 36 m/z were monitored as a function of time to follow the exchange. The m/z values of 28 and 44 were also recorded to check the absence of air or CO_2. The atomic fraction of ^{18}O in the gas phase (α_g), the rate of exchange (R_e), and the number of O atoms exchanged (N_e) were calculated as described in previous references [29]. Typically:

$$\alpha_g = \frac{P_{36} + \frac{1}{2}P_{34}}{P_{36} + P_{34} + P_{32}} \qquad (1)$$

Where P_{36}, P_{34}, and P_{32} were the partial pressures of $^{18}O_2$, $^{18}O^{16}O$, and $^{16}O_2$, respectively;

$$R_e = -N_g \frac{d\alpha_g}{dt} \qquad (2)$$

Where N_g was the number of ^{18}O atoms in gas phase at the beginning of the reaction;

$$N_e = N_g\left(1 - \alpha_g\right) \qquad (3)$$

Finally, the number of exchangeable atoms could be calculated when equilibrium between the gas-phase and the solid was reached by using:

$$N_s = \frac{N_e}{\alpha^*} = N_g\left[\frac{1-\alpha^*}{\alpha^*}\right] \qquad (4)$$

Where α^* was the value of α_g at equilibrium.

Raman spectroscopy

The Raman study was performed using a KAISER RXN1 spectrometer equipped with a NIR (785 nm) laser diode (25< power <50 mW). The powder sample was put in a built-in cell that allowed heating and spectra acquisition under gas flow. Once in the cell, the sample was flushed under a flow of O_2 (50 cm^3 min^{-1}) and heated up to 693 K (5 K min^{-1}) for 1 h. Then, the O_2 flow was switched to Ar (same flow rate), and the cell was cooled down to room temperature (RT), at which point a spectrum was registered. The sample was finally flushed 30 min with O_2 flow (150 cm^3 min^{-1}) at RT, then possibly flushed with an Ar flow (150 cm^3 min^{-1}).

Electron paramagnetic resonance spectroscopy

The EPR spectra were recorded on a JEOL FA-300 series EPR spectrometer at ~9.3 GHz (X-band) using a 100 kHz field modulation and a 2.5 G standard modulation width. The spectra were recorded at 77 K using an insertion Dewar containing liquid nitrogen. Computer simulation of the spectra was performed using the EPRsim32 program [30].

The sample was introduced into a cell consisting of a U-shape reactor with a porous disk for thermal treatment and connected to an EPR tube. The cell can be closed using vacuum valves. After 10 min in dynamic primary vacuum (≈10^{-2} mbar) at RT, 250 mbar O_2 was introduced into the cell, which was then heated at 773 K (5 K min^{-1}) for 2 h. After decreasing the temperature down to 723 K, the sample was evacuated under dynamic primary then secondary vacuum (≈10^{-4} mbar, 10 min) before rapid cooling to RT. At RT, increasing pressures of O_2 were introduced into the cell (from 1.5 up to 50 mbar). After internal transfer of the sample into the EPR tube, the spectra were recorded after 30 min cooling at 77 K (acquisition time: 8 min). The "raw" double integration of the EPR signal (arbitrary units) was performed using the cwEsr software (3.3.36E XB version) provided by JEOL. The double integration per gram of sample, which is proportional to the amount of paramagnetic species in the absence of dipolar interaction, was calculated considering the amount of sample in the EPR tube for each measurement.

Results and discussion

The characterization of the samples studied in this work has been already described in a previous work [7]. The main physicochemical parameters are summarized in Table 1. The BET surface area of pure alumina support slightly decreased as the CeO_2 loading increased, while the high BET surface area of commercial ceria was maintained in the Au/CeO_2 catalyst to 200 m^2 g^{-1}. In $Au/xCeO_2/Al_2O_3$ (x=5 and 10 wt.%), mainly 2-D patches and 3-D nanoparticles of CeO_2 (ca 8 nm) were detected by XRD and EFTEM in accordance with similar observation made by Martínez-Arias [31]. The average sizes of the gold particles visible by EFTEM also reported in Table 1 did not depend on the support but were generally smaller after reduction than after calcination treatment (note that gold particles are visible only on alumina because of the poor contrast between gold and ceria). Finally, XPS and CO oxidation model reaction showed that whatever the mode of activation (thermal treatment under H_2 or O_2), all

Table 1 BET surface area, Au loading, and Au particle size of the catalysts

Catalysts	S_{BET}	Au	Au particle size (nm)	
	(m^2 g^{-1})	(%)	After calcination	After reduction
Au/Al_2O_3	110	0.88	2.4 (0.56)[a]	2.0 (0.49)
$Au/5CeO_2/Al_2O_3$	99	0.89	2.6 (0.43)	2.2 (0.47)
$Au/10CeO_2/Al_2O_3$	92	0.89	2.6 (0.57)	2.0 (0.45)
Au/CeO_2	200	0.97	n.m.[b]	n.m.

[a] Standard deviation is given in brackets

[b] n.m. not measurable

gold was metallic after reduction under H_2, but gold remained unreduced on ceria or ceria patches after calcination under O_2, while it was metallic on alumina.

Oxygen storage capacity

OSC measurements were performed at 673 K. The values obtained for the various samples are reported in Table 2, in which one can distinguish the OSC of the bare supports (denoted "without Au") and the OSC of the samples containing gold (denoted "with Au"). As it could be anticipated, the Al_2O_3 support did not display any OSC activity at 673 K. The activity, i.e., the CO_2 production, remained null for Au/Al_2O_3, confirming the reduced state of gold when deposited on alumina after an oxidation stage at 673 K. Indeed, oxidized gold would have been reduced by the CO pulses, and CO_2 would have been produced. OSC was detectable for $5CeO_2/Al_2O_3$ and $10CeO_2/Al_2O_3$ but was not really different for the two samples. The OSC of bare ceria was much higher, 162 μmol O g^{-1}, corresponding to 0.81 μmol O m^{-2}. In order to assess the proportion of oxygen atoms involved in this process, the latter value was compared with the theoretical one. Taking into account that only one oxygen atom out of four is involved in the Ce^{4+}/Ce^{3+} reduction step, the theoretical OSC for ceria can be estimated as 5.7 μmol O m^{-2}. The ratio between the experimental and theoretical OSC values gives the number of surface oxide layers (N_L) participating to the process. For the bare ceria (200 m^2 g^{-1}), the results in Table 2 show that at 673 K, N_L is restricted to a small fraction of the surface (N_L=0.14). The calculation performed for the ceria of low LSA area shows that N_L is the same (N_L=0.15) and therefore that the OSC process is only dependent on the surface area for a given oxide. In contrast to what was expected, the N_L values were higher when ceria was supported on alumina.

We can notice a beneficial effect of the presence of gold nanoparticles on the OSC values for the various supports (Table 2). On CeO_2, after removing the CO_2 produced by the reduction of oxidized gold, the OSC value was three times as high in the presence of Au. It is worth noting that on CeO_2 LSA, the increase of the OSC by the presence of gold was much lower, showing that the OSC is not only dependent on the ceria surface but also on the Au/CeO_2 interaction. Flytzani-Stephanopoulos et al. also reported the improvement of the OSC property of ceria due to the presence of gold [32]. The impact of Au is more pronounced for the ceria–alumina mixed oxide supports, for which the OSC process involves the participation of bulk oxygen atoms (N_L >1 indicates that the OSC is not limited to the surface) and for which the OSC seems to depend on the CeO_2 content (N_L=1.81 and 2.19 for $Au/5CeO_2/Al_2O_3$ and $Au/10CeO_2/Al_2O_3$, respectively).

Table 2 OSC of $xCeO_2/Al_2O_3$ and CeO_2 at 673 K without or with the presence of 1 wt.% Au

Supports	Without Au		With Au	
	OSC (μmol O g^{-1})	N_L[a]/ CeO_2	OSC (μmol O g^{-1})	N_L/ CeO_2
Al_2O_3	0	0	0	0
$5CeO_2/Al_2O_3$	15	0.53	51	1.81
$10CeO_2/Al_2O_3$	17	0.36	115	2.19
CeO_2 (200 m^2 g^{-1})	162	0.14	474	0.42
CeO_2 LSA (49 m^2 g^{-1})	41	0.15	74	0.26

[a] N_L number of layers; N_L=1 when the surface is entirely involved in the OSC process, N_L>1 when bulk oxygen atoms are involved in the OSC process

Isotopic oxygen exchange ($^{18}O_2/^{16}O_2$ IE)

We first investigated the homo-exchange reaction ($^{16}O_{2(g)}+{}^{18}O_{2(g)} \leftrightarrow 2\ {}^{16}O^{18}O_{(g)}$) by introducing an equimolar mixture of $^{18}O_2/^{16}O_2$ in the Au/CeO_2 system, and the oxygen isotopic exchange evolution was followed in a temperature-programmed experiment. When temperature increased, a decrease of the $^{18}O_2$ partial pressure and an increase of the partial pressures of $^{16}O^{18}O$ and $^{16}O_2$ were observed (Fig. 1). A decrease of the ^{18}O atomic fraction (α_g) was observed in the gas phase when the exchange was taking place. This behavior is not consistent with a homo-exchange reaction during which α_g should remain constant. This result is therefore the indication of a hetero-exchange process in which ^{16}O lattice oxygen atoms, supplied by ceria, participates to the reaction. A very similar evolution of the oxygen isotopomer partial pressures was observed on pure CeO_2 (Fig. S1), meaning that the hetero-exchange is due to ceria. Such a result emphasizes the inability of the gold nanoparticles to dissociatively adsorb molecular dioxygen or shows that the dissociation and the exchange with lattice oxygen atoms occur simultaneously.

In the objective to study whether gold nanoparticles influence the mobility of ceria oxygen atoms or not, we performed

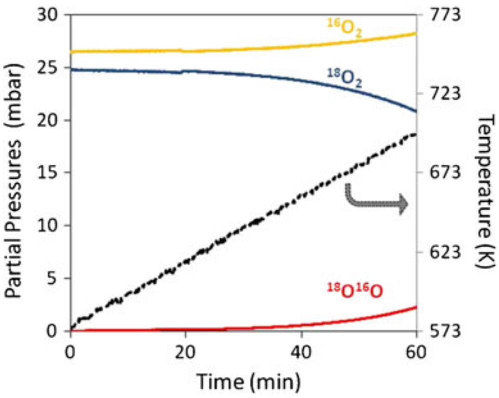

Fig. 1 Evolution of the oxygen isotopomer partial pressures during a tempertaure-programmed homo-exchange experiment on Au/CeO_2 catalyst

an isothermal hetero-exchange experiment, introducing pure $^{18}O_2$ (ca 50 mbar) in the reactor cell at 723 K. The results, in terms of initial rate of exchange (R_e) and number of atoms exchanged (N_e) after 20 min reaction, are reported in Table 3. Again, in this set of experiments, we compared the bare supports (columns denoted "without Au") with the gold catalysts ("with Au"). It clearly appears that the gold nanoparticles exalt the isotopic exchange activity. Since it is well known that Al_2O_3 support is not able to exchange oxygen at 723 K [33], these results show that the exchange is promoted by the interaction between Au nanoparticles and CeO_2. The R_e values, which were low for $5CeO_2/Al_2O_3$ and $10CeO_2/Al_2O_3$, increased in the presence of gold to a value quite similar for both, ca $6–7\times10^{17}$ at O g^{-1} s^{-1}. The similarity between both solids was confirmed in comparing the number of exchanged atoms (Ne values): 5.43 and 5.53 at O nm^{-2} were exchanged for $Au/5CeO_2/Al_2O_3$ and $Au/10CeO_2/Al_2O_3$, respectively, suggesting that the proportion of gold particles in interaction with ceria was close in the two cases. The R_e value normalized per gram of sample was largely higher on bare CeO_2 (55.3×10^{17} at O g^{-1} s^{-1}). Despite this high value, the presence of Au led to an increase of Re (77.8×10^{17} at O g^{-1} s^{-1}). If one examines the Ne values, their increase was not as drastic as for the R_e values (13.7 at O nm^{-2} and 14.7 at O nm^{-2} for CeO_2 and Au/CeO_2, respectively). This can be explained by an equilibrium rapidly reached in the ^{18}O concentration between the gas phase and the solid (depending on the mass of catalyst and the initial pressure of $^{18}O_2$), which minimized the differences that could be detected after 20 min of exchange. Finally, we studied the effect of the ceria surface area with the results obtained on CeO_2 LSA. Contrary to the conclusion previously made regarding the OSC measurement (Table 2), it clearly appears that the oxygen exchange activity is not dependent on the surface area only, since the Ne value, normalized per surface unit, was five times as small for CeO_2 LSA as compared to CeO_2. The beneficial effect of Au was also noticed on CeO_2 LSA, since the R_e and N_e values were almost four times higher in the presence of the metal. Nevertheless, the activity remained smaller than that of the high surface area ceria.

Table 3 $^{18}O_2/^{16}O_2$ isotopic exchange experiments on pre-oxidized samples at 723 K

Supports	Without Au		With Au	
	R_e (10^{17} at O g^{-1} s^{-1})	N_e at 20 min (at O nm^{-2})	R_e (10^{17} at O g^{-1} s^{-1})	N_e at 20 min (at O nm^{-2})
$5CeO_2/Al_2O_3$	1.29	1.06	7.70	5.43
$10CeO_2/Al_2O_3$	1.96	1.61	6.30 (25)[a]	5.53 (10.50)
CeO_2	55.30	13.70	77.80 (183)	14.70 (16.40)
CeO_2 LSA	1.40	2.72	5.40	9.92

[a] Values between parentheses are the results for Au(4 wt.%)/$10CeO_2/Al_2O_3$ and Au(4 wt.%)/CeO_2

In order to ascertain the conclusion that the interaction between Au particles and CeO_2 surface was the key element to explain the strong activity in oxygen exchange, we prepared two other gold catalysts with higher gold loading, i.e., containing 4 wt.% Au deposited on $10CeO_2/Al_2O_3$ and CeO_2. Note that the size of the Au particles was maintained around 2.5 nm. The higher gold loading resulted in higher R_e and N_e values (see values between parentheses in Table 3). A closer inspection of the evolutions of the $^{16}O_2$ (m/z=32) and $^{18}O^{16}O$ (m/z=34) partial pressures as a function of time (Fig. 2) provided possible reasons for the beneficial impact of gold in the oxygen exchange reaction. At the beginning of the reaction, both $^{18}O^{16}O$ and $^{16}O_2$ molecules appeared simultaneously on $10CeO_2/Al_2O_3$ (Fig. 2a) and on ceria support (Fig. 2c). This suggests that simple exchange (Eq. 4) and multiple exchange (Eq. 5) reactions occurred on these supports as already reported for ceria in previous studies [27, 29] as follows:

$$^{18}O_{2(g)}+{}^{16}O_{(s)}\rightarrow{}^{18}O^{16}O_{(g)}+{}^{18}O_{(s)} \tag{4}$$

$$^{18}O_{2(g)}+2\,{}^{16}O_{(s)}\rightarrow{}^{16}O_{2(g)}+2\,{}^{18}O_{(s)} \tag{5}$$

The presence of gold made the $^{16}O_2$ isotopomer the main molecule present at the very beginning of the experiments (Fig. 2b, d), indicating that Au favored the multiple exchange. The promotion of the multiple hetero-exchange mechanism by gold when supported on Ce-doped ordered mesoporous alumina materials has already been reported by Fonseca et al. [34]. Taking into account that the multiple exchange must involve binuclear oxygen species as intermediate, it can be inferred from Fig. 2 that the interfaces between the gold nanoparticles and the ceria crystallites are the preferential location for dioxygen activation, in the form of either diatomic peroxide or superoxide species. The correlation between multiple exchange and peroxide or superoxide intermediate species was suggested by Winter to explain the complex exchange mechanism observed over basic oxides [35]. Corma et al. provided spectroscopic evidences that superoxide species and peroxide adspecies at the one-electron defect site were the active species in the CO oxidation reaction for gold supported on nanocrystalline CeO_2 [36].

To investigate the nature of the binuclear oxygen species adsorbed on the catalytic surface, characterizations by Raman and electron paramagnetic resonance spectroscopies were performed in focusing the study on the impact of the presence of gold nanoparticles.

Identification of oxygen active species

In an attempt to detect undissociated oxygen species by Raman spectroscopy, the catalyst pretreatments were performed in

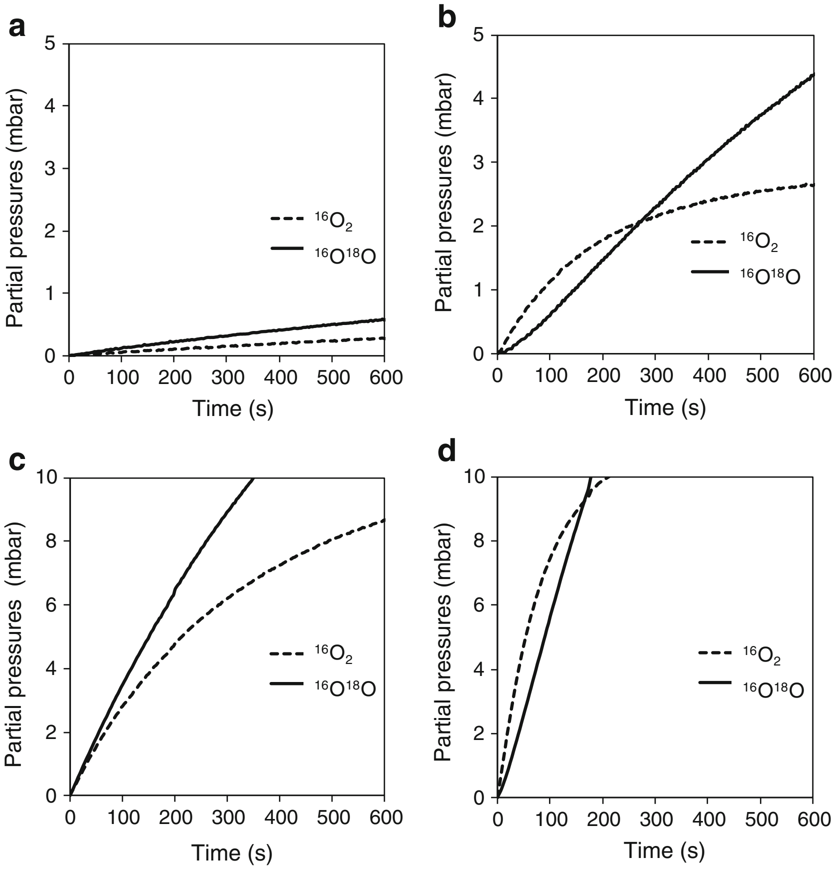

Fig. 2 Evolution of the oxygen isotopomer partial pressures as a function of time during an hetero-exchange experiment at 723 K on **a** $10CeO_2/Al_2O_3$, **b** Au(4 wt.%)/$10CeO_2/Al_2O_3$, **c** CeO_2, and **d** Au(4 wt.%)/CeO_2 catalysts

conditions as close as possible as those used for the isotopic exchange study (see Experimental part). Raman spectroscopy is a sensitive and specific technique capable to discriminate oxygen species (O_2, O_2^- or O_2^{2-}) adsorbed on CeO_2, as reported in earlier works [22, 37]. The vibrational frequencies of these adsorbed oxygen species strongly decrease with their electronic charge; in the 820–890 cm^{-1} range for O_2^{2-} (peroxo), 1,120–1,140 cm^{-1} for O_2^- (superoxo), and 1,480–

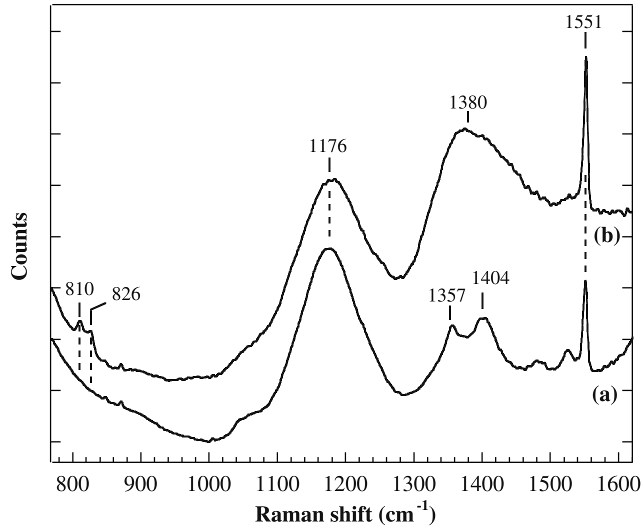

Fig. 3 Raman spectra after calcination at 693 K Ar, then O_2 flow of **a** CeO_2, and **b** Au/CeO_2

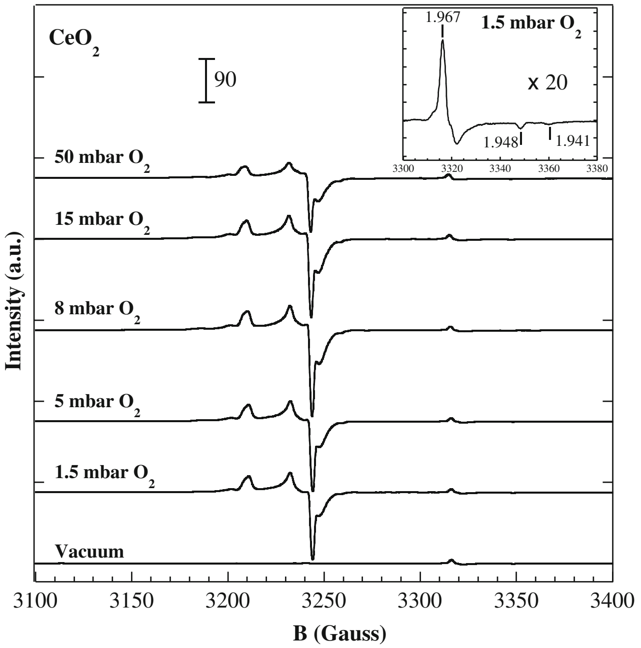

Fig. 4 EPR spectra of CeO_2 sample (recorded after 30 min at 77 K) under increasing PO_2

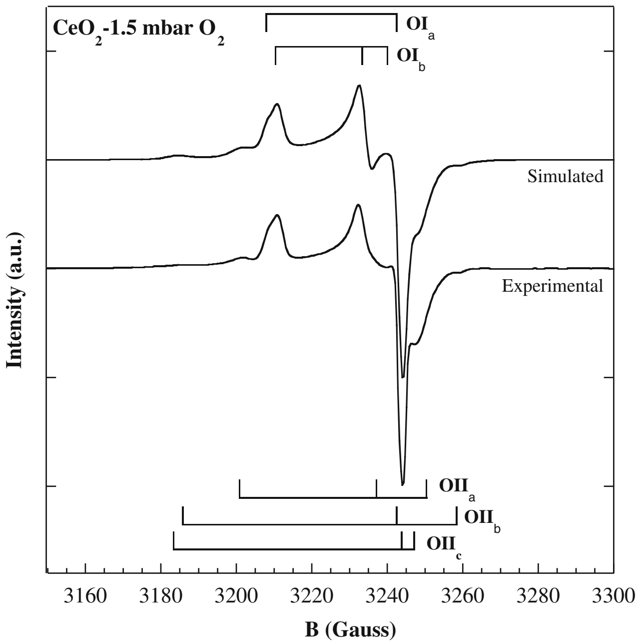

Fig. 5 Experimental (recorded after 30 min at 77 K) and simulated EPR spectra of CeO_2 sample, under 1.5 mbar O_2

1,570 cm^{-1} for physically adsorbed O_2 [22, 37]. Moreover, the resulting bands are sharp compared to the ones related to ceria lattice vibrations, which make them quite easy to identify.

First of all, due to the strong fluorescence of the Al_2O_3-containing materials, only CeO_2 and Au/CeO_2 materials could be studied. Under O_2 flow at RT, apart from the vibration bands characteristic of ceria (Fig. S2), i.e., an intense band at 458 cm^{-1} attributed to 1st order F_{2g} lattice vibrational mode of O_h and weaker bands at 253 and 1,176 cm^{-1} attributed to second order modes, arising from a mixing of A_{1g}, E_g, and F_{2g} lattice vibrational modes [38] (additional bands were visible at 1,357, 1,404, and 1,380 cm^{-1}, assigned to residual carbonate/carboxylate species), the spectra of CeO_2 and Au/CeO_2 (Fig. 3) revealed the presence of a sharp band at 1,551 cm^{-1} that grew under O_2 flow. It can be reasonably attributed to physically adsorbed O_2, since it easily disappeared by flushing with inert gas. One can note that apart from the vibration bands characteristic of ceria described above, a shoulder around 590 cm^{-1} was also visible for both CeO_2 and Au/CeO_2 (Fig. S2). It is related to the presence of oxygen vacancies [39]. The intensity of the 590 cm^{-1} shoulder relative to the F2g mode band (458 cm^{-1}) is about twice as high for Au/CeO_2 (9×10^{-2}) as for CeO_2 (4×10^{-2}), revealing a much more oxygen-defective material in the presence of gold. These additional vacancies are probably located at the perimeter of the interface between gold and ceria and would explain the exaltation of the multiple exchange mechanism observed by isotopic exchange technique for gold-containing catalysts [40]. In addition, tiny bands at 810 and 826 cm^{-1} could be observed on Au/CeO_2 only (not on CeO_2), in the frequency range of adsorbed O_2^{2-} peroxo species. No O_2^- (superoxo) species could be observed. It may be noted that the observation of such superoxo species often requires low temperature (93 K), which could not be reached with our spectrometer. In order to ascertain the presence of O_2^- (superoxo) species, EPR experiments were also performed.

To avoid the interaction between the radical oxygen species and the gas phase O_2 which is known to induce signal broadening, it was necessary to perform the EPR experiments at low temperature, i.e., at the liquid nitrogen temperature, 77 K, which is the usual temperature used for the identification of the oxygen radicals. The EPR study was first performed over CeO_2 and Au/CeO_2. Again, the pretreatments had to be

Table 4 Simulated EPR parameters of O_2^- species adsorbed on CeO_2, Au/CeO_2, $10CeO_2/Al_2O_3$, and $Au/10CeO_2/Al_2O_3$ under 1.5 and 50 mbar O_2

Sample	O_2^- species Assignment*	g_z ($g_{\|\|}$)	g_x ($g_\perp$)	g_y	Proportion (%)	
					1.5 mbar O_2	50 mbar O_2
CeO_2	OI_a	2.033	2.011	2.011	26.5	23.5
	OI_b	2.031	2.017	2.012	30.5	20.5
	OII_a	2.037	2.014	2.007	26.5	27.0
	OII_b	2.047	2.011	2.001	3.5	5.5
	OII_c	2.048	2.010	2.008	13.0	23.5
Au/CeO_2						
	OI_a	2.033	2.011	2.011	48.0	45.5
	OI_b	2.031	2.016	2.011	14.0	16.0
	OII_a	2.036	2.012	2.007	17.0	18.0
	OII_b	2.048	2.011	2.001	1.5	6.5
	OII_c	2.049	2.009	2.008	19.5	14.0
$10CeO_2/Al_2O_3$	OCA	2.027	2.017	2.011	≈100	
$Au/10CeO_2/Al_2O_3$	OCA	2.027	2.017	2.011	≈100	

*According to notations of Martínez-Arias et al. [31]

Table 5 Overall intensity (double integration) of O_2^- species adsorbed on CeO_2, Au/CeO_2, 10CeO_2/Al_2O_3, and Au/10CeO_2/Al_2O_3 upon increasing O_2 pressures

PO_2 (mbar)		1.5	5	8	15	50
Overall intensity	CeO_2	6 590	7 140	9 200	9 060	6 740
	Au/CeO_2	4 070	4 940	6 020	6 220	4 000
	10CeO_2/Al_2O_3	51 300	36 000	29 500	8 350	200
	Au/10CeO_2/Al_2O_3	22 300	8 700	3 800	550	≈0

adapted to the technical constraints, but were performed in conditions as close as possible to those of isotopic exchange (see Experimental part). After treatment under vacuum at 723 K, the EPR spectra of CeO_2 and Au/CeO_2 samples revealed a weak anisotropic signal at $g \approx 1.97$ (Figs. 4 and S3) composed of two species ($g_{\perp 1,2} \approx 1.97$, $g_{\parallel 1}=1.948$, and $g_{\parallel 2}=1.941$, insert of Fig. 4). The signal obtained for Au/CeO_2 was slightly broader because of the presence of a third species ($1.98 < g_{\perp 3} < 1.96$ and $g_{\parallel 3}=1.937$–1.936) (Fig. S3). Its intensity (double integration) was similar for CeO_2 and Au/CeO_2 samples. Though this signal at $g \approx 1.97$ was currently observed on ceria-based samples, its attribution is still under debate. It was tempting to assign it to Ce^{3+}; however, according to the literature, such paramagnetic ion could be observed at very low temperature only (T <20 K) [41, 42]. Some authors proposed that this signal originated from Ce^{3+} in peculiar geometry/symmetry [43, 44], while other authors proposed that it arises from quasi-free electrons with some orbital mixing with the empty f-orbitals of Ce^{4+} ions [23, 45].

Upon addition of O_2, the signal at $g \approx 1.97$ remained unchanged, which further strengthened the hypothesis of a paramagnetic species trapped in the bulk of the CeO_2 particles (no possible dipolar interaction with O_2 that could affect the signal). Moreover, a complex new signal of high intensity appears in the 3,150 G<B<3300 G region, typical of O_2^- species (Fig. 4). It had almost the same shape for CeO_2 and Au/CeO_2 (Fig. S3), and the simulation of the signal (Figs. 5 and S4) indicated the presence of five different O_2^- species in both samples with slightly different proportions (Table 4). The OI's and OII's species have been previously observed on similar materials [46–48]. These species were attributed to different adsorption modes of O_2^- on the surface, OI with EPR-equivalent oxygen atoms (adsorption parallel to the surface), and OII with nonequivalent oxygen atoms (end-on or other asymmetric adsorption).

Upon increasing O_2 pressure, the shape of the O_2^- signal was barely affected, but its intensity increased, then decreased when PO_2>8 mbar and 15 mbar for CeO_2 and Au/CeO_2, respectively, as attested by the values of the double integration reported in Table 5. The decreasing intensity above a critical O_2 pressure probably resulted from dipolar interactions between O_2^- and nearby O_2 molecules [49, 50]. This points out that the O_2^- signal intensity depends not only on the number of paramagnetic species, but also on this broadening effect, thus comparisons of the intensities are meaningful for the smallest O_2 pressures, only. The interesting point regarding these experiments is that the intensity (double integration) of the overall O_2^- signal is smaller for Au/CeO_2 than for CeO_2 (Table 4), indicating that no extra O_2^- species were generated by the presence of gold.

In the case of 10CeO_2/Al_2O_3 and Au/10CeO_2/Al_2O_3, upon O_2 addition, the signal of O_2^- was very different and much more intense at low PO_2 (more than five times) (Fig. 6) than that for CeO_2 and Au/CeO_2 samples (Figs. 4 and S3). Again, the shape of the O_2^- signal was similar for 10CeO_2/Al_2O_3 and Au/10CeO_2/Al_2O_3 (Fig. S5). It was also much less complex than the former ones (Figs. 4 and S3), and could be accurately simulated considering only one O_2^- species, thereafter referred as OCA in the literature [31] (Table 4). It has been proposed that the OI and OII species formed on 3-D CeO_2 nanoparticles, while the OCA species formed on 2-D platelets of CeO_2 [31]. This assignment fits with the fact that CeO_2 consists of 3-D particles, and that, as mentioned at the beginning of the section "Results and discussion", previous EFTEM images of xCeO_2/Al_2O_3 revealed the presence of both 3-D and 2-D (platelets) CeO_2 particles on alumina [7]. The intensity of the OCA species strongly decreased and broadened for O_2 pressures >1.5 mbar, and almost disappeared at $PO_2 \approx 50$ and 15 mbar, for 10CeO_2/Al_2O_3 and Au/10CeO_2/Al_2O_3, respectively, which

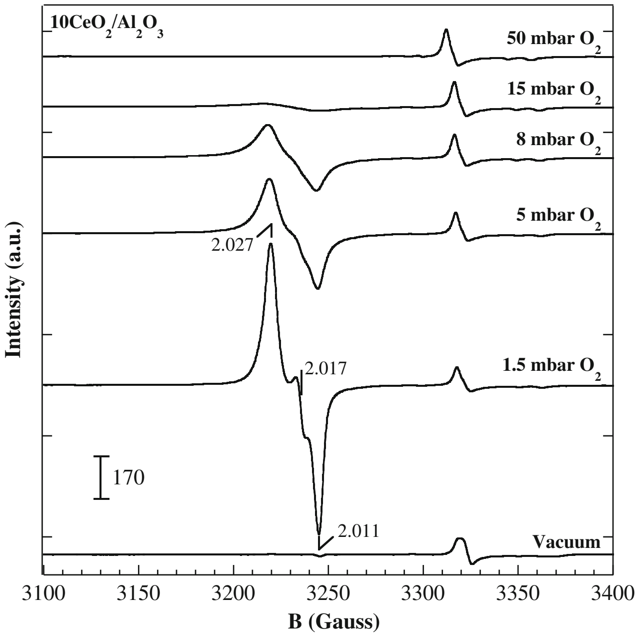

Fig. 6 EPR spectra of 10CeO_2/Al_2O_3 sample (recorded after 30 min at 77 K) under increasing PO_2

was not observed with CeO_2 and Au/CeO_2. Such different behavior towards O_2 dipolar broadening has been reported earlier [51] on CeO_2/SiO_2 and CeO_2/Al_2O_3 materials, and the authors assigned it to the difference in O_2 accessibility to O_2^- species, thus locating O_2^- in the bulk (CeO_2/SiO_2: little to no broadening effect) or on the surface (CeO_2/Al_2O_3: strong broadening effect) of CeO_2. Again, the double integration of the O_2^- signal was somewhat smaller for Au/10CeO_2/Al_2O_3 than for 10CeO_2/Al_2O_3, whatever the pressure of O_2 (Table 5).

To summarize, the comparison of the intensity of EPR signals of O_2^- species in CeO_2 and Au/CeO_2 pointed out a lower amount of O_2^- species in the presence of Au, for which the OSC property and the oxygen isotopic exchange activity was exalted, which ruled out the hypothesis that O_2^- species would play an active role in the corresponding processes. However, the formation of a noticeable amount of O_2^{2-} species adsorbed on Au/CeO_2 and not on CeO_2 strengthened the hypothesis of an activation of dioxygen molecule via Au nanoparticles through the formation of a peroxo species. This interpretation matches the conclusion brought by Pal et al. [18] who reported the results obtained by combining photoelectron spectroscopy and computational method, showing that the O–O bond was more activated (more elongated) in the peroxo form than that in the superoxo one, and suggesting that peroxo mode of chemisorptions plays a crucial role in the dioxygen activation.

Conclusion

In this work, we studied the oxygen mobility and the nature of the oxygenated species responsible for the chemisorption of dioxygen on Au/CeO_2 and Au/xCeO_2/Al_2O_3 ($x=5$ and 10 wt.%) catalysts. We stressed the role of the Au nanoparticles in the step of dioxygen activation. To achieve this goal, oxygen storage capacity measurements and $^{18}O/^{16}O$ isotopic exchange reaction were undertaken to study the oxygen mobility, while Raman spectroscopy and electron paramagnetic resonance spectroscopies were employed to determine the nature and the location of the adsorbed oxygen species. All the characterizations were performed on catalysts previously activated in conditions as close as possible to the thermal pretreatment used prior to the reactions of oxidation studied in our previous work [7].

Au nanoparticles were shown to exalt both the OSC property of CeO_2 and the exchange rate of oxygen between the gas phase and the lattice oxygen atoms of CeO_2, whether the Au nanoparticles were supported on CeO_2 or on CeO_2/Al_2O_3. Complementary results obtained by modifying the gold loading and the ceria surface indicated that the improvement in the oxygen mobility was dependent on the Au/CeO_2 interfacial perimeter. Moreover, the close inspection of the evolutions of the isotopomer partial pressures during the isotopic exchange experiments led to the conclusion that the interfaces between the gold nanoparticles and the ceria crystallites were the preferential location for dioxygen activation via adsorption of binuclear species.

Further characterization by Raman and EPR spectroscopies were performed to determine the nature of the dioxygen species. The study of CeO_2 and Au/CeO_2 by in situ Raman under oxygen revealed the presence of peroxo species on Au/CeO_2 and of additional vacancies probably located at the perimeter of the interface between gold and ceria. EPR revealed the presence of superoxo species on both samples, but their concentration was lower in the presence of gold. The same observation was made for 10CeO_2/Al_2O_3 and Au/10CeO_2/Al_2O_3. As a consequence, the efficiency of Au/CeO_2 and Au/xCeO_2/Al_2O_3 catalysts for oxidation reaction could be explained by the activation of dioxygen molecule at the ceria/Au nanoparticles interfacial perimeter involving peroxo species.

Acknowledgments The authors thank Jean-Marc Krafft, engineer at LRS for the Raman measurements, and Pantea Baripour, master student at LRS for the preliminary experiments of EPR. The authors also acknowledge the Agence Nationale pour la Recherche for financial support (ANR-BLANC07-2 183612).

References

1. Haruta M, Kobayashi T, Sano H, Yamada N (1987) Novel Gold Catalyst for the Oxidation of Carbon Monoxide at a Temperature far below 0 °C. Chem. Lett. 405–408
2. Haruta M, Yamada N, Kobayashi T, Iijima S (1989) Gold catalysts prepared by co-precipitation for low-temperature oxidation of hydrogen and of carbon monoxide. J Catal 115:301–309
3. Bond GC, Louis C, Thompson DT (2006) Catalysis by gold. Imperial College Press, London
4. Fu Q, Saltsburg H, Flytzani-Stephanopoulos M (2003) Active non-metallic Au and Pt species on ceria-based water-gas shift catalysts. Science 301:935–938
5. Leppelt R, Schumacher B, Plzak V, Kinne M, Behm RJ (2006) Kinetics and mechanism of the low-temperature water-gas shift reaction on Au/CeO_2 catalysts in an idealized reaction atmosphere. J Catal 244:137–152
6. Delannoy L, Fajerwerg K, Lakshmanan P, Potvin C, Méthivier C, Louis C (2010) Supported gold catalysts for the decomposition of VOC: Total oxidation of propene in low concentration as model reaction. Appl Catal B Environ 94:117–124
7. Lakshmanan P, Delannoy L, Richard V, Méthivier C, Potvin C, Louis C (2010) Total oxidation of propene over Au/xCeO_2-Al_2O_3 catalysts: Influence of the CeO_2 loading and the activation treatment. Appl Catal B Environ 96:117–125
8. Solsona B, Garcia T, Murillo R, Mastral AM, Ndifor EN, Hetrick CE, Amiridis MD, Taylor SH (2009) Ceria and gold/ceria catalysts for the abatement of polycyclic aromatic hydrocarbons: an in situ DRIFTS study. Top Catal 52:492–500

9. Scire S, Minico S, Crisafulli C, Satriano C, Pistone A (2003) Catalytic combustion of volatile organic compounds on gold/cerium oxide catalysts. Appl Catal B Environ 40:43–49
10. Andreeva D, Petrova P, Sobczak JW, Ilieva L, Abrashev M (2006) Gold supported on ceria and ceria-alumina promoted by molybdena for complete benzene oxidation. Appl Catal B Environ 67:237–245
11. Enache DI, Knight DW, Hutchings GJ (2005) Solvent-free oxidation of primary alcohols to aldehydes using supported gold catalysts. Catal Lett 103:43–52
12. Bion N, Epron F, Moreno M, Mariño F, Duprez D (2008) Preferential oxidation of carbon monoxide in the presence of hydrogen (PROX) over noble metals and transition metal oxides: advantages and drawbacks. Top Catal 51:76–88
13. Carrettin S, Concepcion P, Corma A, Nieto JML, Puntes VF (2004) Nanocrystalline CeO_2 increases the activity of an for CO oxidation by two orders of magnitude. Angew Chem Int Ed 43:2538–2540
14. Widmann D, Leppelt R, Behm RJ (2007) Activation of a Au/CeO_2 catalyst for the CO oxidation reaction by surface oxygen removal/oxygen vacancy formation. J Catal 251:437–442
15. Guan Y, Ligthart DAJM, Pirgon-Galin O, Pieterse JAZ, van Santen RA, Hensen EJM (2011) Gold stabilized by nanostructured ceria supports: nature of the active sites and catalytic performance. Top Catal 54:424–438
16. Hvolbæk B, Janssens TVW, Clausen BS, Falsig H, Christensen CH, Nørskov JK (2007) Catalytic activity of Au nanoparticles. Nano Today 2:14–18
17. Boronat M, Corma A (2010) Oxygen activation on gold nanoparticles: separating the influence of particle size, particle shape and support interaction. Dalton Trans 39:8538–8546
18. Pal R, Wang L-M, Pei Y, Wang L-S, Zeng XC (2012) Unraveling the mechanisms of O_2 activation by size-selected gold clusters: transition from superoxo to peroxo chemisorption. J Am Chem Soc 134:9438–9445
19. Woodham AP, Meijer G, Fielicke A (2013) Charge separation promoted activation of molecular oxygen by neutral gold clusters. J Am Chem Soc 135:1727–1730
20. Green IX, Tang W, Neurock M, Yates JT Jr (2011) Spectroscopic observation of dual catalytic sites during oxidation of CO on a Au/TiO_2 catalyst. Science 333:736–739
21. Yao HC, Yao YFY (1984) Ceria in automotive exhaust catalysts.1. oxygen storage. J Catal 86:254–265
22. Pushkarev VV, Kovalchuk VI, d'Itry JL (2004) Probing defect sites on the CeO_2 surface with dioxygen. J Phys Chem B 108:5341–5348
23. Oliva C, Termignone G, Vatti FP, Forni L, Vishniakov AV (1996) Electron paramagnetic resonance spectra of CeO_2 catalyst for CO oxidation. J Mater Sci 31:149–158
24. Li C, Domen K, Maruya K, Onishi T (1990) Oxygen-exchange reactions over cerium oxide—An FT-IR study. J Catal 123:436–442
25. Li C, Domen K, Maruya K, Onishi T (1989) Dioxygen adsorption on well-outgassed and partially reduced cerium oxide studied by FT-IR. J Am Chem Soc 111:7683–7687
26. Lakshmanan P, Delannoy L, Louis C, Bion N, Tatibouët JM (2013) Au/$x$$CeO_2$/$Al_2O_3$ catalysts for VOC elimination: oxidation of 2-propanol. Catal Sci Technol. doi:10.1039/C3CY00238A
27. Madier Y, Descorme C, Le Govic AM, Duprez D (1999) Oxygen mobility in CeO_2 and $Ce_xZr_{(1-x)}O_2$ Compounds: study by CO transient oxidation and $^{18}O/^{16}O$ isotopic exchange. J Phys Chem 103:10999–11006
28. Ojala S, Bion N, Rijo Gomes S, Keiski RL, Duprez D (2010) Isotopic oxygen exchange over Pd/Al_2O_3 catalyst: study on $C^{18}O_2$ and $^{18}O_2$ exchange. ChemCatChem 2:527–533
29. Duprez D (2006) Oxygen and hydrogen surface mobility in supported metal catalyst. Study by $^{18}O/^{16}O$ and $^{2}H/^{1}H$ exchange. In: Hargreaves JSJ, Jackson SD, Webb G (eds) Isotopes in Heterogeneous Catalysis. Imperial College Press, London, pp 133–181
30. Spalek T, Pietrzyk P, Sojka Z (2005) Application of the genetic algorithm joint with the Powell method to nonlinear least-squares fitting of powder EPR spectra. J Chem Inf Model 45:18–27
31. Martínez-Arias M, Fernández-García M, Salamanca LN, Valenzuela RX, Conesa JC, Soria J (2000) Structural and redox properties of ceria in alumina-supported ceria catalyst supports. J Phys Chem B 104:4038–4046
32. Fu Q, Kudriavtseva S, Saltsburg H, Flytzani-Stephanopoulos M (2003) Gold–ceria catalysts for low-temperature water-gas shift reaction. Chem Eng J 93:41–53
33. Martin D, Duprez D (1996) Mobility of surface species on oxides. 1. isotopic exchange of $^{18}O_2$ with ^{16}O of SiO_2, Al_2O_3, ZrO_2, MgO, CeO_2, and CeO_2-Al_2O_3. Activation by noble metals. Correlation with oxide basicity. J Phys Chem 100:9429–9438
34. Fonseca J, Royer S, Bion N, Pirault-Roy L, do Carmo Rangel M, Duprez D, Epron F (2012) Preferential CO oxidation over nanosized gold catalysts supported on ceria and amorphous ceria-alumina. Appl Catal B Environ 128:10–20
35. Winter ERS (1968) Exchange reactions of oxides. Part IX. J. Chem. Soc. A 2889–2902
36. Guzman J, Carrettin S, Corma A (2005) Spectroscopic evidence for the supply of reactive oxygen during CO oxidation catalyzed by gold supported on nanocrystalline CeO_2. J Am Chem Soc 127:3286–3287
37. Choi YM, Abernathy H, Chen H-T, Lin MC, Lu M (2006) Characterization of O_2–CeO_2 interactions using in situ Raman spectroscopy and first-principle calculations. ChemPhysChem 7:1957–1963
38. Weber WH, Hass KC, McBride JR (1993) Raman study of CeO_2. Second-order scattering, lattice dynamics, and particle-size effects. Phys Rev B 48:178–185
39. McBride JR, Hass KC, Poindexter BD, Weber WH (1994) Raman and x-ray studies of $Ce_{1-x}RE_xO_{2-y}$, where RE=La, Pr, Nd, Eu, Gd, and Tb. J Appl Phys 76:2435–2441
40. Widmann D, Leppelt R, Behm RJ (2007) CO Oxidation activity activation of a Au/CeO_2 catalyst for the CO oxidation reaction by surface oxygen removal/oxygen vacancy formation. J Catal 251:437–442
41. McLaughlan SD, Forrester PA (1966) Orthorombic and trigonal electron-spin-resonance spectra of Ce^{3+} ions in CaF_2. Phys Rev 151:311–314
42. Barrie JD, Momoda LA, Dunn B, Gourier D, Aka G, Vivien D (1990) ESR and optical spectroscopy of Ce^{3+}-β-alumina. J Sol St Chem 86:94–100
43. Dufaux M, Che M, Naccache C (1969) Electron paramagnetic resonance study of oxygen adsorption on supported molybdenum and cerium oxides. Comptes Rendus Acad Sci Paris C86:2255–2257
44. Fierro JLG, Soria J, Sanz J, Rojo JM (1987) Induced changes in ceria by thermal treatments under vacuum or hydrogen. J Sol St Chem 66:154–162
45. Gideoni M, Steinberg M (1972) Study of oxygen sorption on cerium(IV) oxide by electron-spin resonance. J Sol St Chem 4:370–373
46. Mendelovici L, Tzehoval H, Steinberg M (1983) The adsorption of oxygen and nitrous-oxide on platinum ceria catalyst. Appl Surf Sci 17:175–188
47. Soria J, Martínez-Arias A, Conesa JC (1995) Spectroscopic study of oxygen-adsorption as a method to study surface-defects on CeO_2. J Chem Soc Faraday Trans 91:1669–1678
48. Zhang X, Klabunde KJ (1992) Superoxide (O_2^-) on the surface of heat-treated ceria-intermediates in the reversible oxygen to oxide transformation. Inorg Chem 31:1706–1709
49. Povich MJ (1975) Electron-spin resonance oxygen broadening. J Phys Chem 79:1106–1109
50. Pake GE, Tuttle TR (1959) Anomalous loss of resolution of paramagnetic resonance hyperfine structure in liquids. Phys Rev Lett 3:423–425
51. Aboukais A, Zhilinskaya EA, Lamonier JF, Filimonov IN (2005) Colloid Surf A Physicochem Eng Asp 260:199–207